Raman scattering by wave-vector-dependent coupled plasmon/LO-phonon modes in *n*-type InN

YongJin Cho,* Manfred Ramsteiner,† and Oliver Brandt
Paul-Drude-Institut für Festkörperelektronik, Hausvogteiplatz 5–7, 10117 Berlin, Germany
(Received 22 December 2011; revised manuscript received 11 May 2012; published 29 May 2012)

We study the Raman scattering of *n*-type InN films grown by molecular beam epitaxy on ZnO substrates. The observed spectral Raman features are found to strongly depend on the carrier concentration as well as the photon energy used for excitation. The corresponding spectral changes are explained by coupled plasmon/LO-phonon excitations which are influenced by the selective resonance enhancement for scattering at large wave vectors as well as wave-vector nonconservation. In particular, a broad Raman band spanning the whole frequency range of optical phonons is demonstrated to originate from plasmon-related excitations, as opposed to the frequently assumed pure phonon scattering and wave-vector nonconservation induced by structural disorder.

DOI: 10.1103/PhysRevB.85.195209 PACS number(s): 78.30.Fs, 61.72.uj, 63.20.kd

I. INTRODUCTION

Raman spectroscopy is a valuable tool to study epitaxial InN films which, because of the lack of a proper substrate, generally possess high densities of dislocations and unintentional free electrons. Since the doping level is often correlated with the degree of structural disorder,[1] great care has to be taken in the interpretation of Raman spectra. Both structural disorder and heavy doping can lead to similar spectral features. Particularly, a broad Raman band in the range between the transverse optical (TO) and longitudinal optical (LO) phonon frequencies is commonly attributed to pure phonon scattering activated by crystalline defects.[2–5]

The observed line shapes of phonon and plasmon excitations in Raman spectra strongly depend on the accessible scattering wave vectors. For first-order Raman scattering by the deformation potential mechanism in perfect crystals only excitations with very small wave vectors are allowed due to pseudo-momentum conservation. For the understanding of Raman spectra from InN films, however, the following three mechanisms have to be considered as being responsible for first-order Raman scattering with large wave vectors.

(i) Structural disorder is connected with the relaxation of pseudo-momentum conservation for Raman scattering by phonons leading to the observation of broad spectral bands which reflect the density of states and dispersion of acoustic as well as optical phonons, particularly to the above-mentioned broad Raman band in the range between the TO- and LO-phonon frequencies.[2]

(ii) Similarly, elastic scattering of photocreated carriers by ionized impurities in heavily doped materials can lead to a pronounced nonconservation of wave vectors for scattering by plasmon-related excitations.[6]

(iii) For InN, an additional mechanism has been proposed which provides access to large scattering wave vectors in first-order Raman scattering: Double-resonant scattering by the intraband Fröhlich interaction results in a selective enhancement of excitations with a defined large wave vector. As a consequence, the frequency of the LO-phonon line in Raman spectra of InN has been found to strongly depend on the incoming photon energy.[7]

In this paper, we study the impact of *n*-type doping on Raman scattering in epitaxial InN films in which the electron densities and structural qualities are not directly correlated. These samples are thus ideally suited for distinguishing between these three mechanisms.

II. EXPERIMENTAL DETAILS

The *n*-type InN films presented here were directly grown on O-face ZnO(000$\bar{1}$) substrates by plasma-assisted molecular beam epitaxy (PA-MBE). The base pressure of the growth chamber is $< 10^{-10}$ Torr, and the chamber was maintained at $\approx 5 \times 10^{-6}$ Torr during the growth runs. All the InN films were grown under slight N excess with a N/In flux ratio of ≈ 1.2. It has been found that the electron density in these films has a tendency to increase drastically with increasing substrate temperature and with decreasing film thickness presumably because of an interfacial reaction and the resulting incorporation of O donors in the InN films. As a measure of the structural quality of the InN films, we used x-ray diffraction (XRD) ω scans. In particular, the FWHM of the (10$\bar{1}$2) peak reflects the density of edge threading dislocations which are the dominant structural defects in InN films grown by PA-MBE.[8] These FWHM values are listed in Table I for the investigated InN films, together with the substrate temperatures, film thicknesses, and electron densities. Electron densities were estimated via low-temperature photoluminescence[9] and Raman measurements. The electron densities by Raman measurements have been obtained from a line-shape analysis using the approach described, e.g., in Ref. 10. Thereby, we used A_1(TO) and A_1(LO) frequencies of 451.3 and 591.8 cm^{-1} (Ref. 11) as well as a high-frequency

TABLE I. Substrate temperature during InN growth (T_S), film thickness (t), electron density estimated by PL (N_{PL}) and Raman (N_{Raman}) measurements, and FWHM of XRD (10$\bar{1}$2) ω scans (FWHM$_{102}$) for the investigated InN films.

Sample	T_S (°C)	t (nm)	N_{PL} (cm^{-3})	N_{Raman} (cm^{-3})	FWHM$_{102}$ (arcsec)
A	500	1850	6.0×10^{19}	6.6×10^{19}	871
B	475	690	2.1×10^{19}	3.3×10^{19}	1447
C	475	627	5.0×10^{18}	1.2×10^{19}	1239
D	475	2500	3.8×10^{18}	9.5×10^{18}	632

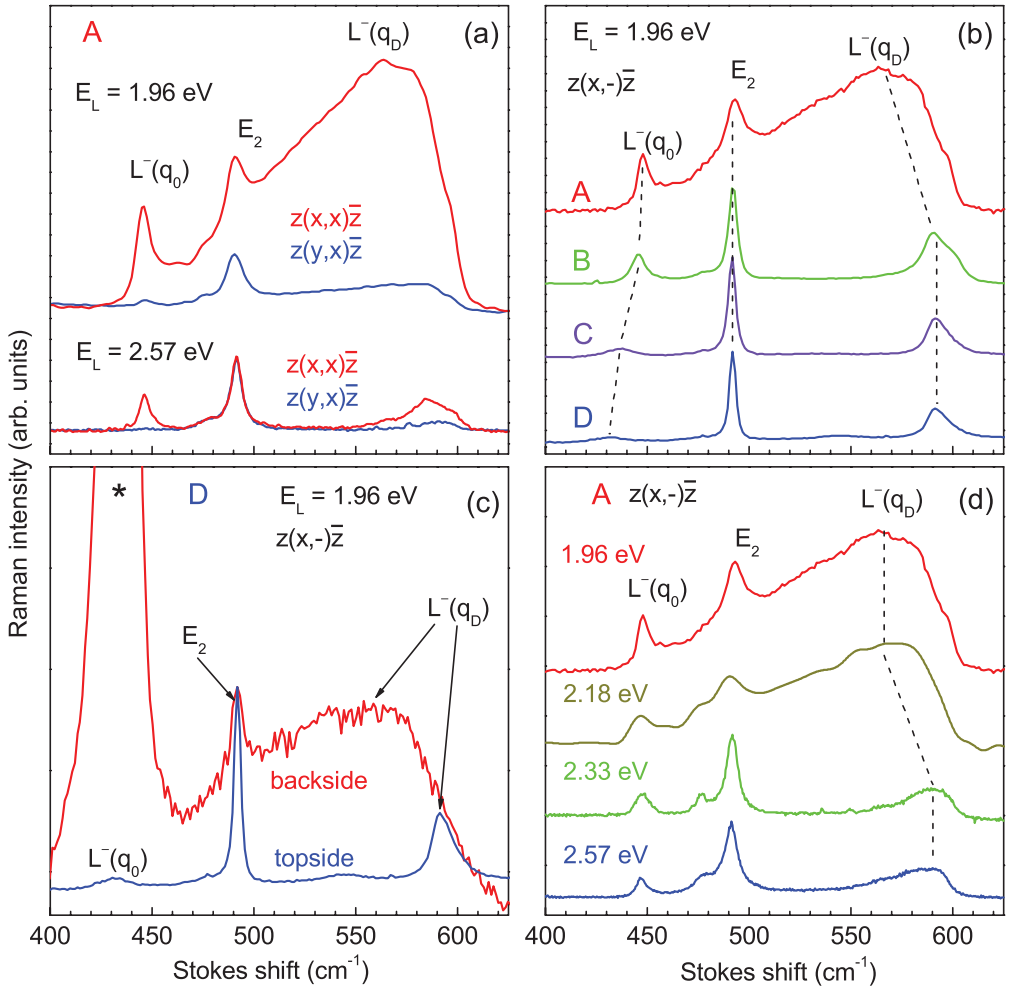

FIG. 1. (Color online) (a) Polarized $[(z(x,x)\bar{z})]$ and depolarized $[(z(y,x)\bar{z})]$ Raman spectra of the heavily doped InN sample A excited at photon energies of 1.96 and 2.57 eV (z is parallel to the c axis of the InN film). (b) Raman spectra of the samples A, B, C, and D(see Table I) excited at a photon energy of $E_L = 1.96$ eV. (c) Raman spectra obtained for backscattering from the topside (blue) and backside (red) of sample D. The asterisk indicates the E_2 phonon frequency of the ZnO substrate. (d) Raman spectra of sample A excited at different photon energies as indicated in the figure. The spectra in (b)–(d) were not analyzed for their polarization, and those in (a)–(d) were vertically shifted for clarity.

dielectric constant of 6.7 (Ref. 12). The nonparabolicity of the conduction band has been taken into account by assuming a parabolic dispersion but different effective masses depending on the doping regime ($0.14m_e$ for sample A, $0.11m_e$ for sample B, and $0.09m_e$ for sample C as well as sample D where m_e is the free electron mass).[13] In order to distinguish the different mechanisms for wave-vector nonconservation, the InN films have been selected in such a manner that the electron densities are comparable in samples C and D whereas the structural quality is similar in samples A and D. Sample B with an intermediate electron density and with the worst structural quality was selected to verify our conclusions. Room-temperature Raman spectra for excitation energies from 1.96 to 2.57 eV were measured using a Jobin Yvon HR-LabRAM spectrograph equipped with a charge-coupled device (CCD) detector. All spectra were measured in backscattering geometry. The optical probing depth for these excitation energies has been determined by room-temperature ellipsometry measurements (not shown here) to lie in the range between 48 and 65 nm.

III. RESULTS

The polarization selection rules for Raman scattering have been investigated for the heavily doped sample A. The corresponding spectra, shown in Fig. 1(a), exhibit three InN-related spectral features peaking at about 450, 491, and 580–590 cm^{-1}. The peak at 491 cm^{-1} is due to the E_2 phonon mode in InN. The Raman features close to the A_1(TO)- and A_1(LO)-phonon frequencies (447 and 580–590 cm^{-1}) may arise from pure phonon scattering[14–16] or excitations related to coupled plasmon/LO-phonon (PLP) modes.[11,17,18] Note that both Raman features exhibit a strong polarization dependence in that they appear dominantly in polarized $[(z(x,x)\bar{z})]$ and only weakly in depolarized $[(z(y,x)\bar{z})]$ spectra. The InN-related Raman features reveal pronounced changes regarding their intensities and spectral shapes when changing the excitation energy from 1.96 and 2.57 eV, but the polarization dependence remains qualitatively the same, as also shown in Fig. 1(a).

The Raman spectra of the InN films depend strongly on the doping level, as shown in Fig. 1(b) for excitation at 1.96 eV.

A very broad and intense Raman feature, labeled $L^-(q_D)$, dominates the spectrum of sample A with the largest electron density and transforms into a much narrower and much weaker Raman feature for samples B, C, and D which are lower doped but, in the case of samples B and C, of worse structural quality (see Table I). In fact, the spectra from the samples with lower electron densities and different structural qualities (samples B, C, and D) are very similar, including a relatively narrow $L^-(q_D)$ peak close to the A_1(LO)-phonon frequency ($\approx$590 cm^{-1}). Note that the same influence of the electron density on the spectral shape of the $L^-(q_D)$ peak has been observed by Thakur *et al.*[14]

Figure 1(c) displays the comparison between Raman spectra acquired in backscattering from the substrate side (backside) and surface side (topside) of sample D. The spectrum obtained from the backside reveals the properties of the region close to the ZnO interface in the InN films, where the electron density induced by the interfacial reaction is expected to be relatively large and eventually comparable to the average concentration in sample A. Indeed, the Raman spectrum of sample D excited from the backside exhibits a broad $L^-(q_D)$ peak which resembles closely that of the heavily doped sample A shown in Fig. 1(b) and deviates strongly from the topside spectrum which exhibits a narrow $L^-(q_D)$ peak close to the A_1(LO)-phonon frequency.

The influence of the excitation photon energy E_L used for excitation on the Raman spectra is shown in more detail in Fig. 1(d) for the heavily doped sample A. The most striking observation is the remarkable change of the $L^-(q_D)$ peak regarding its shape, position, and intensity for photon energies below and above a threshold energy E_t between 2.18 and 2.33 eV. Here, we define E_t as an excitation energy at which the $L^-(q_D)$ peak switches between the two characteristic shapes shown in Fig. 1(d). For photon energies above this threshold, the peak position of the $L^-(q_D)$ peak blueshifts to the A_1(LO)-phonon frequency (580–590 cm^{-1}), becomes considerably narrower, and decreases in intensity. For the lower doped samples B, C, and D, on the other hand, no significant influence of the photon energies on the Raman spectra has been observed (not shown here).

IV. DISCUSSION

To explain all the above experimental findings, we have to consider different Raman scattering mechanisms for phonon- as well as plasmon-related excitations. For the discussion of plasmon-related excitations, we show in Fig. 2(a) the dispersion of the low-frequency PLP mode $L^-(q)$ calculated for an electron density of 6.6×10^{19} cm^{-3} using the approach described above (see Experimental Details). In this calculation we used A_1(TO) and A_1(LO) frequencies of 451.3 and 591.8 cm^{-1}, respectively.[11] The frequency of the $L^-(q)$ mode shifts from a value close to the A_1(TO) frequency at $q = 0$ to that of the A_1(LO) mode at large q values.

Considering the dispersion in Fig. 2(a), it is straightforward to attribute the narrow InN-related Raman peak at about 446 cm^{-1} to the low-frequency PLP mode $L^-(q_0)$ with a small wave vector [$q_0 = 4\pi n_r/\lambda = (4.9\text{–}6.5) \times 10^5$ cm^{-1}, where n_r is the refractive index of InN and λ the laser wavelength] excited via the deformation-potential scattering mechanism.[10,11]

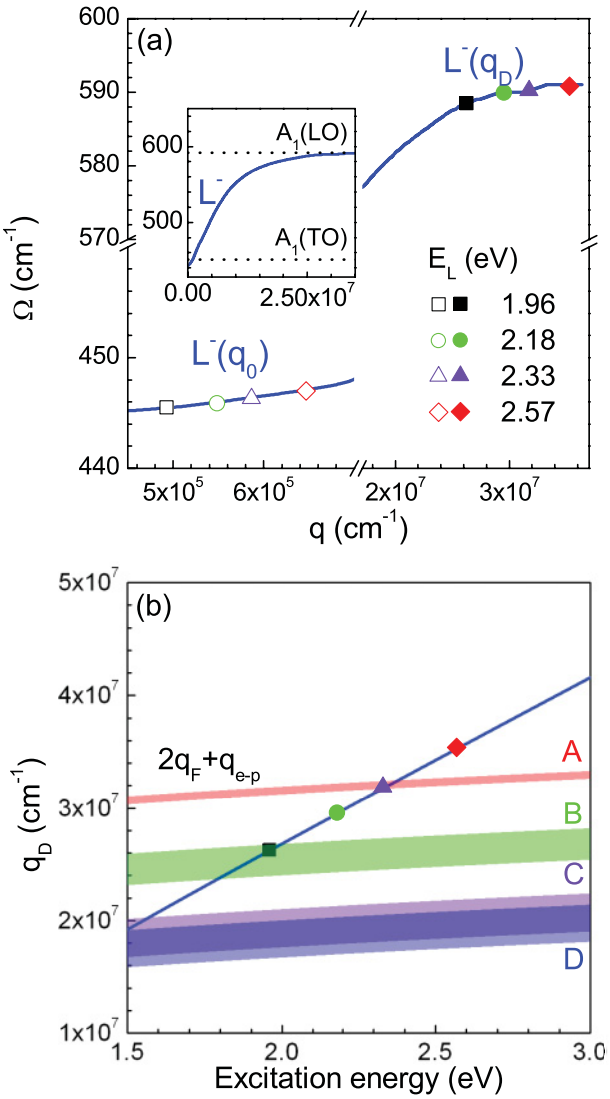

FIG. 2. (Color online) (a) Dispersion of the low-frequency PLP mode $L^-(q)$ calculated for an electron density of 6.6×10^{19} cm^{-3} in the region of scattering wave vectors q_0 (open symbols) and q_D (filled symbols) values for the excitation energies between 1.96 and 2.57 eV. The full dispersion curve of this $L^-(q)$ is shown in the inset. (b) q_D as a function of excitation energy (full line) with the relevant values of the present experiments indicated (filled symbols). The quantity $2q_F + q_{e-p}$ for the investigated samples is indicated by shaded areas. The width of these areas is given by the difference between the electron densities N_{PL} and N_{Raman} (see Table I).

This assignment is supported by the following experimental findings: (1) The observed polarization behavior of the $L^-(q_0)$ peak [see Fig. 1(a)] is expected for PLP modes, but not for pure phonon scattering by the A$_1$(TO) mode.[19] (2) The $L^-(q_0)$ frequency blueshift observed with increasing doping level [see Fig. 1(b)] is quantitatively in reasonable agreement with the electron densities determined by PL measurements (see Table I). (3) The weak dependence of the $L^-(q_0)$ peak frequency on the excitation energy [see Fig. 1(d)] is expected for the low-frequency PLP mode with a small wave vector q_0 at the present doping level [the experimentally observed peak positions coincide with the calculated dispersion shown in Fig. 2(a)].

Regarding the Raman feature $L^-(q_D)$ peaking at 570–580 cm^{-1} and in particular its large spectral width, we have to consider the previously mentioned processes (i)–(iii) leading to first-order Raman scattering with large wave vectors:

(i) Pure phonon scattering with wave-vector nonconservation induced by structural disorder can be excluded as the origin of the broad Raman band in the range between the TO- and LO-phonon frequencies because of the following reasons: (1) The clear adherence to the polarization selection rules [see Fig. 1(a)], (2) the missing correlation with the structural quality [cf. Fig. 1(b) and Table I], and (3) the pronounced change in spectral shape for excitation at large photon energies [see Fig. 1(d)]. Furthermore, even the Raman spectra of samples B and C [see Fig. 1(b)] with the lowest structural qualities (see Table I) exhibit narrow E_2 phonon lines, which is not consistent with pronounced wave-vector nonconservation due to structural disorder.

(ii) Consequently, we attribute the broad Raman feature to plasmon-related excitations which are subject to considerable wave-vector nonconservation induced by the Landau damping (as discussed below) as well as ionized-impurity scattering. With accessible wave vectors in the range between zero and $r \times q_{TF}$ (where q_{TF} is the Thomas-Fermi screening wave vector and r is typically in the range between 1 and 10),[10,14] the dispersion of the PLP mode $L^-(q)$ covers the whole range between the A_1(TO)- and A_1(LO)-phonon frequencies [see Fig. 2(a)].

(iii) To understand the peak position close to that of the A_1(LO)-phonon mode as well as the change in line shape for excitation at larger photon energies ($E_L > E_t$), we have to consider, in addition to wave-vector nonconservation, the double-resonant Raman scattering mechanism by the intraband Fröhlich interaction proposed by Davydov *et al.* for InN films.[7] This resonance enhancement can be observed in a large range of incoming photon energies since in InN a single conduction band with the energy minimum at the Γ point extends from 0.7 up to 4 eV without any additional critical points in this energy interval.[7,20] The underlying mechanism leads to a selective enhancement of Raman scattering with a wave vector q_D given by the photon energy E_L and the electronic band structure: $q_D = 2\sqrt{2\mu(E_L - E_g)/\hbar^2}$, where μ is the reduced effective mass of electrons and light holes, E_g is the fundamental band gap, and $\hbar$ is the reduced Planck's constant.[7] This scattering wave vector is much larger than q_0 which is accessible by conventional first-order Raman scattering, e.g., by the deformation-potential mechanism, and leads eventually to an $L^-(q_D)$ mode which is essentially phonon-like, i.e., fully unscreened and decoupled from excitations of the free carrier gas. This transition occurs at the upper boundary of the Landau damping regime, i.e., when following condition is fulfilled:[7]

$$q_D > 2q_F + q_{e-p}. \tag{1}$$

Here q_F is the Fermi wave vector and q_{e-p} given by $\sqrt{2m^*\Omega_{LO}/\hbar}$ with the electron effective mass m^* and the wave-vector dependent A_1(LO)-phonon frequency Ω_{LO}.[7] For the phonon-like $L^-(q_D)$ mode which occurs under the above condition, the wave-vector nonconservation is assumed to be strongly reduced, since the uncertainty of q_D is determined by the decay of electron-hole pairs in intermediate states[7] and is likely to be affected by the Landau damping as well as by ionized-impurity scattering. As a result, the corresponding Raman peak is expected to be located close to the A_1(LO)-phonon frequency with a relatively small linewidth [see Fig. 2(a)], as experimentally observed for samples B, C, and D [see Fig. 1(b)] and for sample A at $E_L > E_t$ [see Fig. 1(d)]. The apparent shift of the $L^-(q_D)$ peak observed in Fig. 1(d) is a result of the q dependence in the Raman scattering efficiency inside the range of accessible wave vectors (below and above the wave vector q_D).

The dependence of q_D on the excitation energy E_L is shown in Fig. 2(b) together with the quantity $2q_F + q_{e-p}$ (with nonparabolicities of conduction and valence bands taken into account)[7,21] for the investigated samples. Regarding samples B, C, and D, the above condition indeed seems to be fulfilled for all excitation energies used for this study [filled symbols in Fig. 2(b)]. Furthermore, the observation of an unscreened phonon-like $L^-(q_D)$ mode from sample A is expected only for excitation energies $E_L > 2.3$ eV. The slight discrepancies between experiments [Fig. 1(d)] and calculations [Fig. 2(b)] observed in samples A ($E_L = 2.33$ eV) and B ($E_L = 1.96$ eV) might be due to uncertainties of estimated electron densities. In this way, the experimentally observed line shapes of the $L^-(q_D)$ mode in the different samples as well as their dependence on the excitation energy [see Figs. 1(b) and 1(d)] are exactly explained by regarding the transition from inside to outside the Landau damping regime which is given by the above condition and illustrated in Fig. 2(b).

The Raman efficiency for the double-resonant Fröhlich scattering mechanism is expected to be proportional to the doping density.[7,22] Indeed, the ratio between the integrated intensity of the $L^-(q_D)$ peak (normalized to that of the E_2 phonon peak) and the doping density N_{Raman} (see Table I) is found to be nearly constant at $(0.55 \pm 0.10) \times 10^{-18}$ cm^3 for samples B, C, and D. The larger ratio of 2.45×10^{-18} cm^3 found for sample A with $E_L = 1.96$ eV is most likely due to the wave-vector nonconservation which leads to a very broad $L^-(q_D)$ peak [see Fig. 1(b)]. In fact, for $E_L = 2.57$ eV, under the condition of suppressed wave-vector nonconservation, the ratio between the intensity of the unscreened phonon-like $L^-(q_D)$ peak and N_{Raman} is similar for all samples. This observation supports our above explanation of the different line shapes in the Raman spectra of n-type InN and their dependence on the excitation energy.

V. CONCLUSIONS

We have demonstrated the influence of selectively enhanced scattering at large wave vectors as well as wave-vector nonconservation on the Raman spectra from n-type InN films. The remarkable spectral changes induced by an increasing doping level as well as by a variation of the excitation energy can only be explained by plasmon-related Raman scattering. In this framework, the wave-vector nonconservation is induced by ionized-impurity scattering and not by structural disorder as frequently assumed.

ACKNOWLEDGMENTS

The authors are indebted to Hans-Peter Schönherr for the maintenance of the MBE system and to Snežana Lazić for critical reading of the manuscript.

*Present address: Department of Applied Physics, Eindhoven University of Technology, 5600 MB Eindhoven, The Netherlands; yjcho@alumni.nd.edu
†ramsteiner@pdi-berlin.de

[1] L. F. J. Piper, T. D. Veal, C. F. McConville, L. Hai, and W. J. Schaff, Appl. Phys. Lett. **88**, 252109 (2006).
[2] Z. G. Qian, W. Z. Shen, H. Ogawa, and Q. X. Guo, J. Appl. Phys. **93**, 2643 (2003).
[3] V. V. Mamutin, V. A. Vekshin, V. Yu. Davydov, V. V. Ratnikov, T. V. Shubina, S. V. Ivanov, P. S. Kopev, M. Karlsteen, U. Sderwall, and M. Willander, Phys. Status Solidi A **176**, 247 (1999).
[4] M. Kuball, J. W. Pomeroy, M. Wintrebert-Fouquet, K. S. A. Butcher, H. Lu, and W. J. Schaff, J. Cryst. Growth **269**, 59 (2004).
[5] V. Yu. Davydov and A. A. Klochikhin, Semiconductors **38**, 861 (2004).
[6] G. Abstreiter, M. Cardona, and A. Pinczuk, in *Light Scattering in Solids IV*, edited by M. Cardona and G. Güntherodt (Springer, Berlin, 1984), p. 5.
[7] V. Yu. Davydov, A. A. Klochikhin, A. N. Smirnov, I. Y. Strashkova, A. S. Krylov, H. Lu, W. J. Schaff, H.-M. Lee, Y.-L. Hong, and S. Gwo, Phys. Rev. B **80**, 081204(R) (2009).
[8] C. S. Gallinat, G. Koblmüller, F. Wu, and J. S. Speck, J. Appl. Phys. **107**, 053517 (2010).
[9] M. Moret, S. Ruffenach, O. Briot, and B. Gil, Appl. Phys. Lett. **95**, 031910 (2009).
[10] F. Demangeot, C. Pinquier, J. Frandon, M. Gaio, O. Briot, B. Maleyre, S. Ruffenach, and B. Gil, Phys. Rev. B **71**, 104305 (2005).
[11] V. Yu. Davydov, V. V. Emtsev, I. N. Goncharuk, A. N. Smirnov, V. D. Petrikov, V. V. Mamutin, V. A. Vekshin, and S. V. Ivanov, Appl. Phys. Lett. **75**, 3297 (1999).
[12] A. Kasic, E. Valcheva, B. Monemar, H. Lu, and W. J. Schaff, Phys. Rev. B **70**, 115217 (2004).
[13] J. Wu, W. Walukiewicz, W. Shan, K. M. Yu, J. W. Ager, E. E. Haller, H. Lu, and W. J. Schaff, Phys. Rev. B **66**, 201403 (2002).
[14] J. S. Thakur, D. Haddad, V. M. Naik, R. Naik, G. W. Auner, H. Lu, and W. J. Schaff, Phys. Rev. B **71**, 115203 (2005).
[15] T. Inushima, M. Higashiwaki, and T. Matsui, Phys. Rev. B **68**, 235204 (2003).
[16] A. Kasic, M. Schubert, Y. Saito, Y. Nanishi, and G. Wagner, Phys. Rev. B **65**, 115206 (2002).
[17] R. Cuscó, J. Ibáñez, E. Alarcón-Lladó, L. Artús, T. Yamaguchi, and Y. Nanishi, Phys. Rev. B **79**, 155210 (2009).
[18] Y. M. Chang, H. W. Chu, C. H. Shen, H. Y. Chen, and S. Gwo, Appl. Phys. Lett. **90**, 072111 (2007).
[19] H. Harima, J. Phys.: Condens. Matter **14**, R967 (2002).
[20] R. Goldhahn, P. Schley, A. T. Winzer, M. Rakel, C. Cobet, N. Esser, H. Lu, and W. J. Schaff, J. Cryst. Growth **288**, 273 (2006).
[21] A. A. Klochikhin, V. Yu. Davydov, I. Y. Strashkova, and S. Gwo, Phys. Rev. B **76**, 235325 (2007).
[22] V. Yu. Davydov, A. A. Klochikhin, M. B. Smirnov, Y. E. Kitaev, A. N. Smirnov, E. Y. Lundina, H. Lu, W. J. Schaff, H.-M. Lee, H.-W. Lin, Y.-L. Hong, and S. Gwo, Phys. Status Solidi C **5**, 1648 (2008).